Fringe Image Enhancing in the Light Wavelength Stepping Method

Leszek Chmielewski
and
Marek Skłodowski Waldemar Cudny Mariusz Nieniewski
Adam Kuriański Bogdan Michalski
EPSILON Applied Research Group Co.Ltd.
Daniłowiczowska 11/66, PL 00-084 Warsaw

Abstract Images used for the Light Wavelength Stepping Method (LWSM), obtained in white light and with random dot patterns, are different from typical fringe images because of their 'grainy' texture and untypical sparseness of fringes. For these images the traditional fringe-oriented methods of image enhancement which rely on the directional and repetitive structure of an image fail. Hence, three other methods have been adapted and tested: adaptive median filtering, image enhancement based on estimated Markov model, and image enhancement based on weak membrane model. While the results are satisfying for all of them, the smoothing capability of the Markov and membrane methods, the contrast preserving feature of the adaptive median filter, and the edge preserving capability of the membrane method have to be emphasized. A procedure for equalizing and enhancing the contrast of a fringe image has been proposed and evaluated. From the underlying study a conclusion concerning the position of fringes in real images can be drawn.

Key words: fringe images, image enhancing, speckle methods, Light Wave Stepping Method, fringe image equalizing.

1. Introduction: Fringe images in the Light Wavelength Stepping Method

This paper presents results of experiments with enhancing the white light speckle fringe images. The reason of the interest in these particular fringe images was our studies on the Light Wavelength Stepping Method (LWSM). A detailed description of this promising method is given in [23] and [24]. In the following only a short explanation of the method is presented.

The LWSM is used for measuring the phase (or fringe order) in interferometric images. The surface of an object to be measured is prepared by covering it with a dot pattern ([2]). Two images are taken: one of the deformed object and one of the undeformed object which is used as a reference. These two images are obtained with white light and then they are analyzed in an appropriate optical system with a polychromatic light source. The results of this analysis take the form of three images, each of them corresponding to a different light wavelength. Typically these images are referred to as the red, green, and

blue images, respectively. These images are formed with speckles which result from the interference phenomena in the optical system. The speckles are of different brightness and are organized into fringes. Therefore, the images can be referred to as both the speckle and the fringe images, and each of these descriptions underlines one of the features: the 'graininess' or the periodicity. The fundamental feature of these output images is that if the dots with which the measured object is covered are random, then a fringe in the image is a collection of points representing equal displacement in the direction determined by the layout of the optical system. The scaling factor which relates the fringe order (number) to the displacement value is different for each of the three images. This feature makes it possible to calculate the displacement field of the imaged object, even without knowing the fringe orders in the red, green, and blue images.

The LWSM is related to the Phase Stepping Method (PSM) ([11, 15]), but differs from it in that instead of using three images obtained with three strictly related light phase values (PSM), three images generated with three different light wavelengths are utilized (LWSM).

A lot has already been said about enhancing various kinds of images, among them the fringe images (see for example [15]). Why should white light speckle images be treated separately? The reason lies in some of their features:

- The structure of the images under consideration is 'grainy'. This effect is due to the physical process of image formation, and is a result of irregularities and microscratches on the object surface. This kind of texture should rather be smoothed out than removed altogether.
- The carrier frequency in the image is low; in other words, the fringes are sparse, and their contrast is low. This is particularly typical for images obtained by means of random dot patterns.
- The majority of images are dark. On the one hand, the physical dimensions of the light source in the analyzing system should be small enough so that this source could be considered as a point source. On the other hand, if the AD converter sensitivity is too high, strong electronic noise is introduced.
- Impurities of the optical system and reflexes from the object surface give rise to light flashes.

The LWSM should be insensitive to at least some of the above mentioned image features, similarly as it is the case with the PSM. However, it can be anticipated that an appropriate image enhancement method would rather improve the overall performance of the LWSM. Moreover, some of the operations on a poor-quality image are impossible to be performed automatically, even if they are relatively easy for a human operator. A good example for this is fringe ridge following in a noisy environment. In such a case, a good image enhancement method can transform a 'difficult' image into a one which can successfully undergo automatic treatment.

Another important factor is better readability of the enhanced images for humans.

From the above, the following conclusions can be drawn:

- The required degree of image modification is relatively large.
- There is no sufficiently repetitive structure in the image which could be used for image enhancement.
- It is difficult to separate the elimination of spurious artefacts, like light flashes on impurities of the optical system, and the smoothing of the graininess in the image.

It will be demonstrated in the Section 2.4 how a method giving very good results for fringe images in general, fails in the special case of white light speckle images. This method is based on a lowpass adaptive Fourier filter using a sophisticated method of direction finding (Section 2.1.2). The failure of this method made us look for other approaches. The methods considered in this paper are the following: the relatively simple and fast adaptive median filtering, the image enhancement based on estimated Markov model, and the image enhancement using the weak membrane model. According to the authors' knowledge, the last two methods have never been applied to the processing of fringe images. Finally, a numerical method of equalizing and enhancing the contrast of fringes in an image will be presented.

The paper is organized as follows. First the methods of image enhancement are presented (Sections 2.1-2.3). Then the results obtained with these methods are compared on the basis of a set of example images (Section 2.4). Finally, the fringe contrast enhancement method is described and its preliminary evaluation is carried out (Section 3).

In the following, single-authored sections are marked with the initials of the respective authors.

2. Image enhancement methods

2.1. Adaptive Directional Filtering (MN)

A fringe image represents objects which have a distinct directional feature. By analogy with representation of mountain ranges in topographical maps, where the lines of constant altitude give the information about the slope of the mountains, the lines of constant grey level in the fringe image give the information about the slopes of the fringes. This is a valuable information which can be used along with the data on the position of local maxima and minima corresponding to the ridges and valleys in the mountainous landscape. Enhancement of the fringe images consists in filtering which should remove noise and leave the shape of the fringes intact. It follows from this assumption that the filtering should take place along the direction of the fringe rather than in the direction of the greatest variability of the grey level function, which forms a right angle to the ridge of the fringe. The idea of the adaptive filter for fringe images was taken from [13], where fingerprint filter design is presented. The fingerprint images depict strongly directional objects, and in this sense they are similar to fringe images. However, designing the filters

for fingerprint images is somewhat simpler, since the variability of the ridges and valleys in the fingerprint image is relatively limited and can be specified with reasonable accuracy. In particular, the specification for the fingerprint image filter includes the minimum and maximum width of the ridge, minimum and maximum width of the valley, and the minimum radius of curvature of the ridge. The filtering in [13] is performed in the spatial domain by convolution of the original image with a mask of size $M \times M$, where M - natural number. The basic assumptions relative to the fingerprint image filter are the following:

1. The filter should increase the contrast between the ridge and the valley.
2. Ridge enhancement should follow the local orientation of the ridges.
3. The contrast enhancement should depend only on local differences in intensities.
4. The filter mask should cover at least one period of the signal, that is one ridge and one valley. The mask should be large enough to average out noise; however, it should not be so large as to average across the local changes in the curvature.
5. The filter should be symmetric about its axis of orientation.

In the case of the fringe image filter only the assumptions (2), (3), and (5) can be maintained. Increasing the contrast between the ridge and the valley would distort the information about the slopes of the fringe. The images assumed for the analysis are typically of size 256×256 with 256 grey levels. The number of fringes in a single image is greater than three and less than 10. Under these circumstances the mask straddling the whole period of the signal, that is one ridge and one valley, would be of excessive size.

The use of the adaptive directional filters seems a reasonable choice for the enhancement of fringe images. As it has been shown above, directionality of the filter helps preserve the shape of the slopes. However, since the direction of the fringes changes, the filter should adapt itself to the local direction of the fringe.

2.1.1. Adaptive Median Filtering

The adaptive median filter finds the local direction of the greatest variability of the grey level function by calculating the gradient of the function which approximates the grey level function over the mask. In the computer program developed, one can choose the size of the mask, which can be 3×3, 5×5, 7×7, or 9×9.

As an approximation of the grey level function, the equation of the plane was assumed in the form

$$z = \alpha x + \beta y + \gamma \tag{1}$$

where α, β, γ - unknown coefficients; x, y - coordinates of a pixel, z - grey level at a pixel (Fig. 1).

The gradient of the function given by the right-hand side of Eq. (1) determines the direction of the greatest variability of the grey level function in the image.

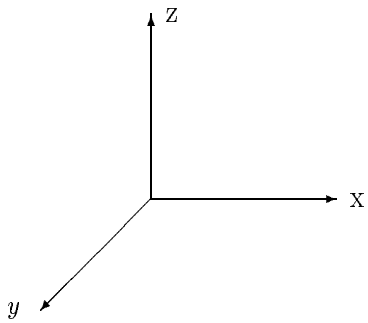

Fig. 1. x, y, z axes.

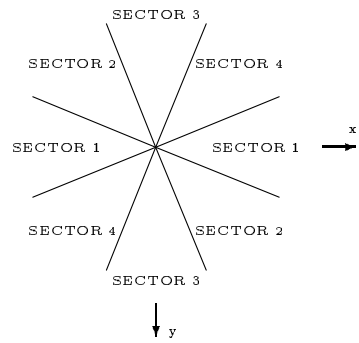

Fig. 2. The sectors of constant filter mask orientation.

In order to fit the plane to the grey values obtained for the mask positioned on any pixel in the image, one uses the criterion of minimization of the sum of squares of differences of the actual grey values z_i at the pixels and the values calculated by substitutions into Eq. (1)

$$\sum_{i=0}^{i=n^2-1} (z_i - \alpha x_i - \beta y_i - \gamma)^2 \tag{2}$$

where n - number of pixels in the mask.

Differentiating expression (2) with respect to α, β, γ and setting the derivatives equal to zero gives the following equations

$$\sum x_i^2 \alpha + \sum x_i y_i \beta + \sum x_i \gamma = \sum x_i z_i \tag{3}$$

$$\sum x_i y_i \alpha + \sum y_i^2 \beta + \sum y_i \gamma = \sum y_i z_i \tag{4}$$

$$\sum x_i \alpha + \sum y_i \beta + n\gamma = \sum z_i \tag{5}$$

The coefficients α, β, γ are found from the set of Eqs. (3)-(5) by means of the determinants, provided that the characteristic determinant of this set is different from zero. The gradient of the function defined by Eq. (1) is a vector with two components: α and β, and its direction is given by the angle

$$\phi = \tan^{-1}\left(\frac{\beta}{\alpha}\right) \tag{6}$$

with respect to the x-axis.

For simplicity reasons, it was assumed that the angle ϕ can only change in steps and is equal to zero or to a multiple of 45°, measured with respect to the x-axis. This means that any value of ϕ is to be rounded to the nearest multiple of 45° so that one obtains four sectors in the x, y plane, each sector being defined by two appropriate multiples of 45° (Fig. 2).

For each sector the filtering is performed in the direction perpendicular to the axis of the sector. The output value of the grey level function at a given pixel is found as a median from the mask centred on the pixel considered and consisting of several pixels located along a straight line. In the program described the size of the mask can be chosen to be 3, 5, 7, or 9.

It is known that the median filter is effective in the case of impulsive noise, and in this particular case it removes impulsive noise in the direction along the ridge of the fringe.

2.1.2. Adaptive Fourier Filtering

Image enhancement is also possible by means of the adaptive directional Fourier filter. The algorithm presented below is based in part on [8]. The Fourier filtering under consideration includes, similarly to the adaptive median filtering, two stages: determination of the direction of the greatest variability of the grey level function, and Fourier filtering with the mask rotated perpendicularly to the direction of the greatest variability.

Determination of the direction of the greatest variability based directly on the original image would be greatly influenced by the noise in the image. In order to reduce the noise influence, the original image is filtered by means of the Gaussian filter. The Gaussian filtering is used in this case exclusively for the purposes of finding the direction of the greatest variability of the grey level function. The aim of the Fourier filtering, which is performed at a later stage, is the calculation of the grey level values in the output image.

The transfer function of a typical low-pass Gaussian filter can be described by the following equation in polar coordinates:

$$F_1(r,\theta) = e^{-\frac{1}{2}r^2\sigma^2}, \tag{7}$$

where σ is a filter parameter (dispersion), r - radius, θ - angle with respect to x-axis. In fact, the Gaussian filter is rotationally symmetric and its transfer function is independent of the angle θ. It can be argued that the orientation of the fringe image filter should be insensitive to very low frequencies representing changes of the grey level function due to varying lighting conditions of the background. This leads one to a conclusion that the Gaussian filter should consist of two F_1 filters differing in the sign and the dispersion. Hence the overall transfer function of the used filter is

$$F_2(r,\theta) = e^{-\frac{1}{2}r^2\sigma_1^2} - e^{-\frac{1}{2}r^2\sigma_2^2} \tag{8}$$

The F_2 filter passes the frequencies in the band determined by the parameters σ_1 and σ_2. The impulse response of the F_2 filter is

$$f_2(x,y) = \frac{1}{2\pi}\left(\frac{1}{\sigma_1^2}e^{-\frac{x^2+y^2}{2\sigma_1^2}} - \frac{1}{\sigma_2^2}e^{-\frac{x^2+y^2}{2\sigma_2^2}}\right) \stackrel{def}{=} H(x,y) \tag{9}$$

The program described performs filtering by calculating the convolution of a given image I with the impulse response H of the filter (Eq. 9). This operation can be represented by the equation

$$C = H * I \tag{10}$$

where C - image obtained by Gaussian filtering.

It is now necessary to find the direction of the greatest variability for the filtered image. It would seem that taking the gradient of the grey level function in this image

$$\nabla(H * I) \tag{11}$$

would give the direction of the greatest variability of the grey level function at each pixel. However, the Gaussian filtering may not give entirely satisfactory results with the effect that the computations of gradients would still be contaminated by noise. The calculation of the greatest variability of the grey level function can be further improved upon by averaging out the computations of gradients.

Theoretically, it is possible to find the directional derivative of the grey level function as a function of the angle θ at every pixel of the image, determine the angle of the greatest variability of the grey level function, and finally find the grey value in the output image. Performing these operations involves a large amount of computations. However, the problem is alleviated by the following considerations.

The directional derivative for any angle θ can be found at any pixel by substituting into the expression

$$[\cos\theta,\ \sin\theta] \cdot \nabla(H * I) \tag{12}$$

where the dot in the above expression stands for the inner product of the vectors $[\cos\theta,\ \sin\theta]$ and $\nabla(H * I)$. In order to proceed further, one defines a function $V(\theta)$, which is equal to the convolution of a certain mask W with the squares of magnitudes of directional derivatives

$$V(\theta) = W * \{[\cos\theta,\ \sin\theta] \cdot \nabla\,(H * I)\}^2 \tag{13}$$

The mask W is used in order to average out the calculations of the gray level variability over certain area. In the simplest case all the weights in the mask W are equal. Equation (13) can also be written in the form

$$V(\theta) = W * \{C_x \cos\theta + C_y \sin\theta\}^2 \tag{14}$$

where C_x and C_y denote the derivatives of C in the direction of x- and y-axis. It can be proved ([8]) that the angle ϕ of the greatest variability of the grey level function is

$$\phi = \frac{1}{2}\tan^{-1}\left(\frac{W * 2C_xC_y}{W * (C_x^2 - C_y^2)}\right) \tag{15}$$

The constants $\sigma_1 \leq 2$ and $\sigma_2 \leq 4$ are chosen by the user of the described program. The program adjusts the size of the mask for the Gaussian filter by setting it to $M \times M$, where $M \geq [(2\sigma_2) + 1]/3$. The mask W for averaging the magnitudes of gradients is of constant size 9×9.

Once the direction of the greatest variability of the grey level function has been established, the program filters the input image using the directional Fourier transform. For this purpose the mask of a typical size 16×16 is used, after being rotated by angle

ϕ. Figure 3 shows in detail how the mask is rotated. The particular size of the mask is chosen to make possible calculation of the FFT, which means that M has to be a power of 2. As exemplified by Fig. 3, the pixels of the rotated mask do not coincide with the pixels of the image so that it is necessary to somehow relate the grey values of the pixels in the mask to the grey values of the pixels in the image. The approach used in the algorithm described is the following. Suppose the mask is in its original position with the center B of the mask at the point A (Fig. 3) and it is desired to find the filtered value of the grey level function in the pixel lying in the NE direction relative to the point A. For this purpose one moves the center B to the middle of the pixel considered and rotates the mask appropriately. In a general case the center of any pixel of the mask, for example the point C in Fig. 3, falls on a certain pixel in the image. It is assumed that the grey value at pixel C is equal to the grey value at this particular pixel of the image. In the relatively rare cases when the point C falls on the border between the pixels the grey value at pixel C is taken arbitrarily from the pixels sharing this common border.

For the mask in which the grey values are specified as f_{kl}, where $k, l = 0, 1, \ldots M-1$, the values F_{mn} of the Fourier transform for $m, n = 0, 1, \ldots M-1$ can be written as

$$F_{mn} = \sum_{k=0}^{M-1} \sum_{l=0}^{M-1} f_{kl} e^{-2\pi i(km+ln)/M} \tag{16}$$

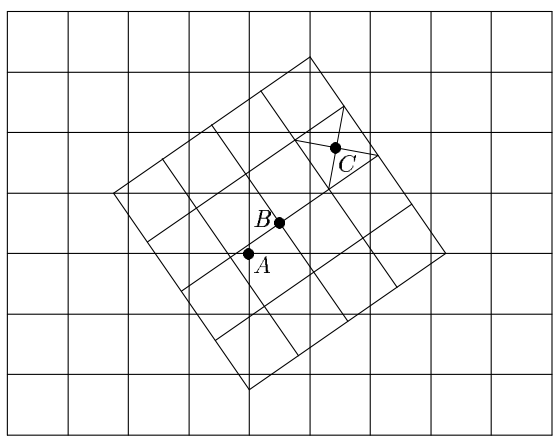

Fig. 3. Mask of the Fourier filter.

The filtering is performed in the direction perpendicular to the direction of the greatest variability of the grey level function. Assume that the values F_{mn} are arranged into

the array

$$\begin{matrix} F_{0,0} & F_{0,1} & \dots & F_{0,15} \\ & & \ddots & \\ F_{15,0} & F_{15,1} & \dots & F_{15,15} \end{matrix}$$

and that the vertical direction in this array corresponds to the direction of the greatest variability. In this case only the values in the first few rows, for example two rows

$$\begin{matrix} F_{0,0} & F_{0,1} & \dots & F_{0,15} \\ F_{1,0} & F_{1,1} & \dots & F_{1,15} \end{matrix}$$

are maintained and the rest is dropped. The particular number of the maintained rows can be set by the user of the program. The inverse transform is then calculated by using the equation

$$f_{kl} = \frac{1}{M^2} \sum_{k=0}^{M-1} \sum_{l=0}^{M-1} F_{mn} e^{2\pi i(km+ln)/M]} \tag{17}$$

Checking again Fig. 3 one finds that there are four pixels in the mask which overlap the pixel which lies in the NE direction relative to the point A in the image. It is assumed that the grey value of this pixel in the image is equal to the average of the four grey values of the pixels adjoining the central point B in the mask.

The presented version of the adaptive Fourier filter can effectively remove the noise from a fringe image.

2.2. Image enhancement based on estimated Markov model (AK)

2.2.1. Introduction

Markov random fields (MRFs) are the mathematical models of grey level functions, used in many algorithms of computer vision ([6, 10, 18]). They belong to the statistical or mixed (deterministic-statistical) group of models of computer images ([21, 22]) and are based on probability theory. The common feature of all statistical models of grey level functions is their ability of noise reduction.

The image enhancement algorithm based on the estimated Markov model of the image uses the approach originally presented in [10] and is denoted as the Gaussian-Logistic-Gradient Markov Field Model. This algorithm was later developed and modified in [21]. In the following, only the outline of the method is presented.

2.2.2. Hierarchical Gaussian-Logistic-Gradient Markov field model

Hierarchical MRF models are suitable for image enhancement and restoration ([22]). The hierarchical MRF contains two layers: the *upper layer* and the *lower layer* ([10]). The upper layer represents the grey level function, whereas the lower layer represents the edge elements in the image. The idea of edge elements was introduced in [5]. According to this concept, a vertical or horizontal edge exists at a site between two neighbouring

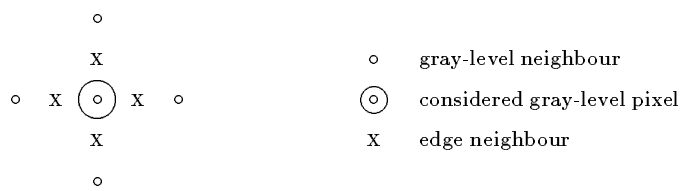

Fig. 4. Neighbours of a considered grey level pixel.

pixels of the grey level upper layer in a given row or a column on condition that the difference of the grey levels of the involved pixels is 'high enough'.

In order to use the estimated Markov model, one has to choose the energy function of Gibbs distribution ([3]). For a one-layer MRF, the energy function is simply a sum of clique potentials ([5, 21]). In the multilayer models, the choice of the energy is more complex. A mutual influence of the layers is to be taken into account. This influence is expressed by means of the consistency energy or conditional potentials ([21, 22]).

The choice of the energy function determines local characteristics of the MRF. In many problems the local characteristics are chosen initially and then the energy function is found ([1, 4, 6, 22]).

In further considerations the following notation is used:

X_i – one-dimensional random variable at pixel i;
x_i – realization of the random variable X_i;
$\boldsymbol{X}$ – multidimensional random variable representing the whole image;
$\boldsymbol{x}$ – realization of the random variable $\boldsymbol{X}$.

It is assumed in the described method that the degraded image is simply a sum of the original noiseless image and of white noise

$$\boldsymbol{Y} = \boldsymbol{X} + \boldsymbol{N}$$

where:
$\boldsymbol{X}$ – original image (before degradation);
$\boldsymbol{N}$ – white noise with constant variance;
$\boldsymbol{Y}$ – random field of observation.

The original image $\boldsymbol{X}$ is modelled by a hierarchical MRF. For both layers, the first order neighbourhood model is chosen (Figs. 4 and 5). In this model a grey level pixel has four grey level neighbours and also four edge neighbours, whereas an edge pixel has six edge neighbours and two grey level neighbours.

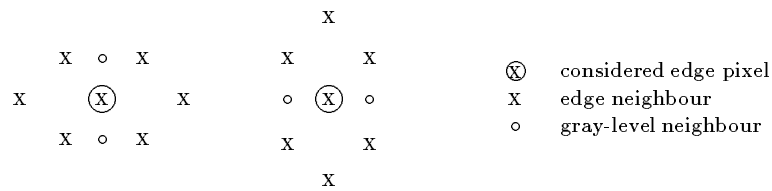

Fig. 5. Neighbours of a horizontal (left) and a vertical (right) edge pixel.

2.2.3. Local characteristics and energy function

The assumed local characteristics of the grey level field are Gaussian distributions with the mean value depending on neighbours of a given pixel and with a constant variance. In such a case the total energy $U_g(\boldsymbol{x})$ of a grey level field can be written as:

$$U_g(\boldsymbol{x}) = \alpha_1 \sum_{i \in S_g} (x_i - \mu_X)^2 + \alpha_2 \sum_{(i,j) \in S_g} (x_i - \mu_X)(x_j - \mu_X)$$

where:

$\boldsymbol{x}$ – realization of the multidimensional random variable modelling the grey level field;

x_i – realization of the one-dimensional random variable representing the grey value at a given pixel;

$\mu_X = E[x_i]$ – mean value of the random variable X_i;

S_g – domain of the grey level field;

(i, j) – pair of pixels belonging to S_g such that j is the neighbour of i;

α_1, α_2 – parameters of the grey level field energy.

In [10] for local characteristics of the edge field the Bernoulli distribution was chosen with its parameter Θ depending on the neighbours. This means that the neighbouring pixels exert influence on the considered pixel via the parameter Θ.

The total energy function $U_e(\boldsymbol{\xi})$ of such an edge field has the form

$$\begin{aligned} U_e(\boldsymbol{\xi}) \;=\; & \lambda_1 \sum_{k \in S_e} \xi_k + \lambda_2 \sum_{(k_1,k_2) \in S_e} \xi_{k_1}\xi_{k_2} + \lambda_3 \sum_{[k_1,k_2] \in S_e} \xi_{k_1}\xi_{k_2} + \\ & \lambda_4 \sum_{(k_1,k_2,k_3) \in S_e} \xi_{k_1}\xi_{k_2}\xi_{k_3} + \lambda_5 \sum_{(k_1,k_2,k_3,k_4) \in S_e} \xi_{k_1}\xi_{k_2}\xi_{k_3}\xi_{k_4} \end{aligned} \tag{18}$$

where:

$\boldsymbol{\xi}$ – realization of the multidimensional random variable modeling the edge field;

ξ_i – realization of the one-dimensional random variable representing an edge at a given site;

S_e – domain of the edge field;

$\lambda_1, \ldots, \lambda_5$ – parameters of the edge field energy, i.e. potentials of every kind of clique;

(k_1, k_2) – two-pixel diagonal edge clique;
$[k_1, k_2]$ – two-pixel horizontal or vertical edge clique;
(k_1, k_2, k_3) – three-pixel edge clique;
(k_1, k_2, k_3, k_4) – four-pixel edge clique.

The consistency energy of both fields is assumed in the form

$$U_{ge}(\boldsymbol{x}, \boldsymbol{\xi}) = -\Delta^2 \sum_{(i,j)\in S_g} (x_i - x_j)^2 \xi_{k_{(i,j)}}$$

where:

$k_{(i,j)}$ – edge between i and j grey level pixels;

Δ^2 – parameter of the consistency energy which represents the mutual influence of the edge and the grey level fields (the greater the value, the higer dependency of two layers is observed).

The total energy of the chosen hierarchical two-layer MRF is

$$U(\boldsymbol{x}, \boldsymbol{\xi}) = U_g(\boldsymbol{x}) + U_e(\boldsymbol{\xi}) + U_{ge}(\boldsymbol{x}, \boldsymbol{\xi}) \tag{19}$$

2.2.4. Estimation of the parameters of the MRF

The following parameters have been introduced in the Markov model: α_1, α_2, Δ^2 and $\boldsymbol{\lambda}$, where vector $\boldsymbol{\lambda} = (\lambda_1, \lambda_2, \lambda_3, \lambda_4, \lambda_5)$. The α_1, α_2 are the parameters of the grey level field, $\boldsymbol{\lambda}$ is the parameter of the edge field, and Δ^2 is a parameter of the consistency energy.

In order to estimate the parameters of the model two problems have to be solved.

1. The noise variance should be determined.
2. Some typical realization of the edge field corresponding to the image to be enhanced has to be found.

In [10] instead of noise variance the parameter $R \in [0, 1]$ called *the inverse signal-to-noise ratio coefficient* is used. This is the first parameter of the presented method. If $R \to 1$ smoothed images are obtained.

In order to obtain a typical realization of the edge field, the *narrow alternative edge detector* ([21]) is used. The operation of this detector for the vertical edge site is illustrated by Fig. 6. The threshold of the detector is the second parameter of the presented method. If the threshold is too low, then many spurious edge elements are found. If the threshold is too high, then the edge elements can not be detected and the image to be enhanced is oversmoothed. ([21]).

Having obtained the edge field realization and the value of the coefficient R, one can estimate the parameters α_1, α_2, Δ^2 and $\boldsymbol{\lambda}$ ([10]). An improved method of estimating $\boldsymbol{\lambda}$ is given in [21].

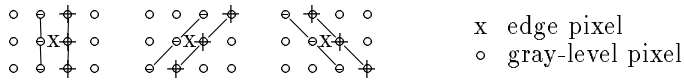

Fig. 6. Detection of vertical edges.

2.2.5. Estimating the parameters of Markov model

Once the local characteristics and their parameters have been found, the Markov model of the image can be obtained by using the Maximum à Posteriori (MAP) method of estimating the underlying noiseless image. In the described procedure, the simulated annealing was used for the MAP. In order to save the computation time the exponentially decreasing temperature function

$$t(k) = vr^k$$

was chosen, where k – current iteration number, $r \leq 0.5$, and $v \leq 0.95$. Because of the rapidly changing temperature, the MAP procedure should be called 'freezing' rather than 'annealing'.

2.2.6. Experimental results

Numerous experiments were made. The best results of image enhancement were obtained, when there were no edges in the image and the freezing algorithm was terminated approximately after ten iterations. This case corresponds to the oversmoothing of the image. The use of freezing caused that only the local minima of the energy function were found. This dificulty was overcome by initializing the freezing with the observed noisy image.

The performed experiments allowed us to conclude that in the case of speckle images the best results are obtained if the method is insensitive to the initial edge realization. This means that the original method from [10] is unuseful for the enhancement of the speckle images. In order to avoid the introduction of a new model we decided to modify the original one. The influence of the edge elements on the solution is reduced by the third parameter called the *smoothing parameter*. This parameter is defined as a Boolean variable. In order to minimize the dependency of the grey-level layer and the edge layer, it is enough to set the third parameter to TRUE. Then the image is locally smoothed by averaging immediately after the initial edge detection and before annealing. If this is the case, the initial edge field realization does not match the grey level image. As a result, the edges disappear during the annealing and the MAP estimate of the Markov model is oversmoothed ([21]).

2.3. Image enhancement based on the 'weak membrane' model (LC)

The weak membrane image enhancement method is described in detail in [7]. The overview given here[1] is sufficient for the purposes of using the algorithm and not for an analysis of its operation.

The method fulfils two tasks simultaneously:

- elimination of high-frequency noise
- detection of edges, defined as sets (or strings) of interpixel boundaries across which large grey level differences between neighbouring pixels occur.

The tasks are fulfilled by minimizing some function E, defined on the input image $d(x, y)$ and the output image $u(x, y)$, $x, y \in S$, where S is the (discrete) domain of the input as well as of the output image

$$E = \sum_{x,y \in S} (u(x, y) - d(x, y))^2 + \lambda^2 \sum_{x,y \in S} grad^2[u(x, y)] + \alpha \sum_{dl \in L} dl \tag{20}$$

In the above equation λ and α are the parameters of the energy function, and L is the locus of interpixel boundaries of length dl in the image. The gradient is approximated by a difference scheme.

The function E can be considered as the energy of an elastic membrane, with its shape (out-of-plane deflection) described by $u(x, y)$. The membrane is attached to an elastic base, the initial shape of which is described by $d(x, y)$. λ represents the ratio of stiffnesses of the membrane and the base. The membrane can break, and the energy of the break of unit length is proportional to α. A break represents an edge in the image. It appears if the energy of the broken membrane is less than that of the continuous one, which depends on the ratio α/λ^2.

The functional (20) is minimised with an iteration algorithm called the *graduate non-convexity* algorithm, described in detail in [7]. That algorithm caters for finding the global minimum and avoids sticking to the local ones. For a typical case about 50 to 80 iterations are necessary (more for larger λ).

The parameters λ and α play the following role. λ is the scale of the filter; if the membrane were compared to the Gaussian filter, λ would be an analog of 3σ, that is the 'influence range' of the filter. The degree to which the high-frequency components are attenuated in the image increases with λ. The parameter α is responsible for the minimum height of a detectable edge in the input image: a straight, isolated edge will be detected if its height is not less than

$$h_0 = \sqrt{2\alpha/\lambda} \tag{21}$$

The threshold h_0 is valid only for edges which are far from each other with respect to the scale λ; the nearer two edges the larger is the threshold. Also, steep slopes may give

[1] The non-invariant version of the algorithm with fixed edge threshold has been applied.
[2] The problem of dimensions of λ and α is omitted here, similarly as was the case in [7].

rise to edges if the grey level gradient is larger than

$$h_1 = \sqrt{\alpha/2\lambda^3} \tag{22}$$

Double edge occurs if the gradient is larger than

$$h_2 = 2\sqrt{\alpha} \tag{23}$$

In practice, λ and h_0 are considered as algorithm parameters. λ should be chosen large enough to provide for sufficient filtering, and not too large to avoid false edges formation (h_1). False edges can be avoided if α and h_0 are large; if the membrane is to be broken, however, h_0 should be kept small enough.

Now let us remind the advantages and disadvantages of the weak membrane image enhancement method. This will be done by comparison to the typical edge-finding and filtering algorithms based on image blurring and maximum gradient detection, such as the Laplacian-of-Gaussian.

The following advantages can be listed:

1. Edges are found in the process of image enhancement; this nonlinear optimization procedure yields excellent edge stability independently of the scale parameter λ. In contrast, the Laplacian-of-Gaussian filter dislocates the edges if the gradient of the grey level function is not symmetrical with respect to the edge, with the dislocation proportional to the scale.
2. Edges in the image are very well preserved since there is no 'filtering across the edges'; also the joints do not fall apart, which does happen when blurring is used in typical filters.
3. The points 1 and 2 hold also for noisy images.
4. The iterative algorithm is formulated so that the area of the output image is the same as that of the input image, irrespective of the scaling parameter. As a result, very large values of λ can be used. In contrast, filters performing convolution of the image with a mask do not allow positioning the mask center too close to the image boundary since the mask takes some space.
5. The algorithm can deal with sparse data in a natural way: the first term in Eq. (20) is omitted for pixels where no data are provided, and the grey levels of the output image $u(x, y)$ are interpolated for these pixels. As a result, some regions can be excluded from fitting to the input image data $d(x, y)$; for example, evident defects can be eliminated (see Figs. 43 and 45 in Section 3.4).

The disadvantages are the following:

1. The optimization algorithm based on Eq. (20) tends to generate uniform grey level regions separated by edges in the output image[3].
2. Edge sensitivity depends on the mutual layout of the edges.

[3] A much more time-consuming algorithm based on the weak plate model does not have this disadvantage ([7, 25]).

3. False edges are found if the slope of the grey level function is large[4]
4. The algorithm is relatively time-consuming, and the time of calculations grows rapidly with λ[5].

The main reason for the interest in the weak membrane method of fringe image enhancement is the possibility of setting the scaling parameter to arbitrarily large values. Investigation of the images presented in Section 2.4 reveals that not only high-frequency noise is the problem, but also the image granularity, fringe unevenness, and occurring discontinuities. The size of these defects lies in the range from a single pixel to tens of pixels.

In the images representing thin objects the half-width of the appropriate Gaussian filter can be comparable to the object dimension. This results in the loss of information in the majority of the object area. In such cases also the edge-preserving feature of the membrane is of vital importance.

The edge finding property and the satisfactory performance in the vicinity of the sharp edges also proved to be an important feature of the described method, although false edges can become a severe problem in images with higher fringe density.

The major difficulty when using the method is its tendency to reduce the gradients of the grey level image. This limits the range of acceptable λ.

The results obtained so far with the image enhancement method using the weak membrane model seem quite satisfactory. However, the above mentioned tendency to reduce the gradient, prompted the authors to start investigations of the weak plate model ([25]).

2.4. Comparison of the enhancement methods

All the analyzed images which are presented below were obtained from physical experiments. In the case considered it seems impossible to apply the standard procedure of evaluating the filtering methods by adding noise to a reference image, filtering the noise out, and comparing the result with the reference. Anything like a reference, 'pure', or 'theoretical' image does not exist, although the images obtained in the experiments vary in quality within certain bounds. Therefore, evaluation of the image enhancement will be carried out via a set of selected image examples ([17]), and the conclusions will be based on the evaluation of the results by human experts.

Examples of the original images used by the image enhancement procedures are shown in Figs. 7, 11, 13, 17, 19, 21, and 23.

All of the test were performed on images with 256 grey levels.

The images of Figs. 17 and 19 represent two special cases of a rotation followed by

[4] The 'invariant' version which reduces the grey level gradient more significantly can alleviate this problem ([16]).

[5] see calculation times given in figure captions in Section 2.4

a translation of a rigid object. These images were obtained with regular dot patterns, but the fringes can be considered as those for random pattern images of a very good quality and adequate average dot distance. All the remaining images are the random dot images. Fig. 21 shows a typical image of the displacement state in a buckled plate fixed on one edge and subjected to an in-plane point load on the other[6]. Fig. 13 shows the *longitudinal* component of the displacement of a cantilever beam[7]. There is only one full fringe in this figure, and the quality of this image is exceptionally poor because of a very coarse texture and numerous false artefacts (reflexes).

The images of Figs. 11, 13, 17, 19, and 21 were obtained with a green light sensor of a colour CCD camera ([20]). The remaining two original images show the blue (Fig. 7) and the red (Fig. 23) component of a fringe image representing transversal displacement of a cantilever beam. The images contain three almost vertical fringes which can be seen much more distinctly in Fig. 23 than in Fig. 7. Disregarding the difference of brightness, careful analysis reveals that the fringe positions in the two images are slightly different. This is expected, as the maximum sensitivity of the blue and red light camera sensors appear at different wave lengths.

Finally, there is an image which will be excluded from the current analysis: Fig. 11. It was obtained in the same way as those of Figs. 17 and 19, but the fringe density as high as in this image could hardly be obtained with the random dot speckle method in white light.

In the preceding Sections the following four fringe image enhancement methods were described:

Adaptive median filter (Section 2.1.1).

Adaptive Fourier filter (Section 2.1.2).

Method based on the estimated Markov model (Section 2.2).

Method using the weak membrane model (Section 2.3).

The Fourier filter seems to be the most 'classic' approach to enhancing fringe images ([9, 15]). The advanced method of estimating the local fringe direction should even add extra strength to it. However, the experiments give clear evidence that it is not so.

Let us compare the image of Fig. 7 with its filtered counterparts in Figs. 8, 9 and 10, obtained with various parameters (see figure captions). It can be seen in the first processed image that instead of enhanced fringes, a fibrous texture showed up. This texture represents local directional features of the grainy texture which can be found in the original image in Fig. 7 under careful examination. In order to minimize the fibrous effect the masks used in subsequent images were made significantly larger. However, in the second image the same effect is present, but the resulting texture exhibits a stronger longitudinal tendency. In the third image the parameters of the direction finder were

[6] As this image was very dark, for presentation it has been slightly brightened by a linear shift in its grey scale. The same concerns the filtered version of the image in Fig. 22.

[7] Due to the requirements of the optical analysis system the image is rotated by 90°.

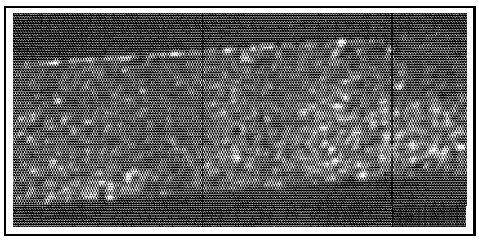

Fig. 7. Transversal displacement of a cantilever beam, blue component - the original 256×120 image for experiments with the Fourier filter.

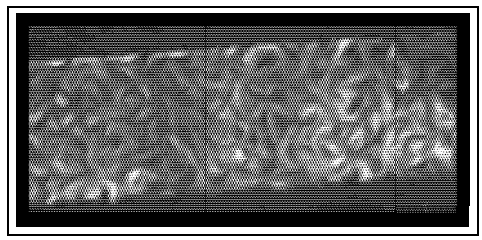

Fig. 8. Image of Fig. 7 after adaptive Fourier filtering; 9×9 masks for gradient averaging and direction estimation; 16×16 mask for the Fourier transform; $\sigma_1 = 2$; $\sigma_2 = 4$; number of the maintained rows in the inverse transform $N = 2$. Calculation time ≈ 18 min.

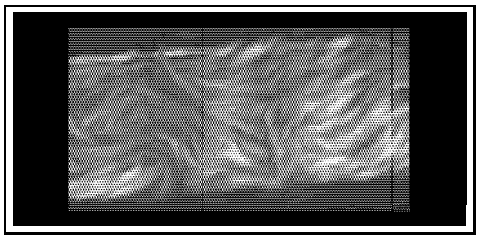

Fig. 9. Image of Fig. 7 after adaptive Fourier filtering. 33×33 masks for gradient averaging and direction estimation; 32×32 mask for the Fourier transform; $\sigma_1 = 3$, $\sigma_2 = 10$, $N = 2$. Time ≈ 75 min.

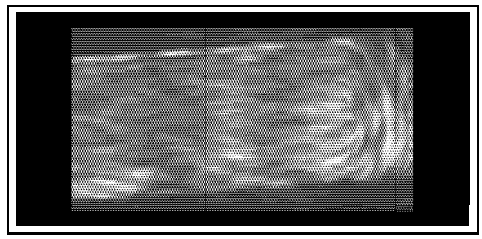

Fig. 10. Image of Fig. 7 after adaptive Fourier filtering; the masks are the same as for Fig. 9. $\sigma_1 = 6$, $\sigma_2 = 20$, $N = 2$. Time ≈ 100 min.

changed to detect the larger-scale gradient, but then the direction of the object as a whole dominated over the directionality of the fringes.

The time of calculation for the three enhanced images was significant and increased rapidly with the scaling parameter of the filter[8]. As the adaptive Fourier filter appeared to be unsuitable for fringe image enhancement, no attempt was made to make its algorithm more effective, although it is evident that with a relatively small effort the time of calculation could have been greatly reduced.

The described experiments illustrate the difficulties with the large scale directional filters encountered when the fringe density is low, as is a typical case with white light random dot speckle images. With higher density of the fringes, the adaptive Fourier filter

[8] All the times of calculations, given in the image captions, were measured for an AT 80486DX, 50MHz computer. The software was written in Borland C++ v. 3.0.

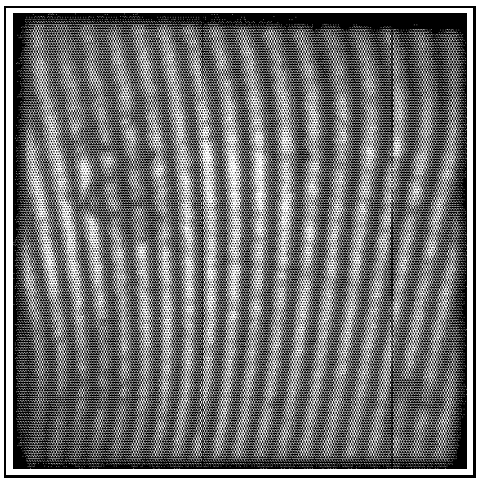

Fig. 11. Rotation and translation of a rigid object - the original 256 × 256 image.

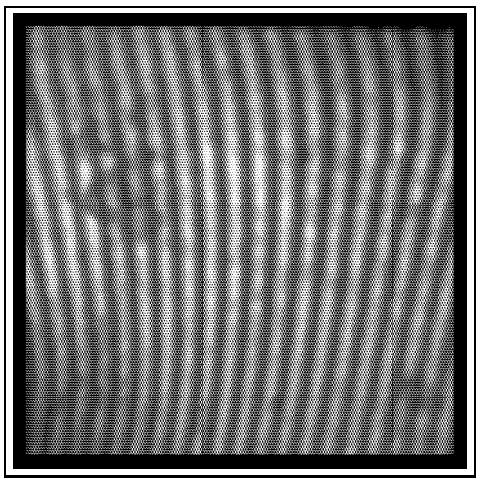

Fig. 12. Image of Fig. 11 after adaptive Fourier filtering, with good result. Parameters as for the image of Fig. 8. Time ≈ 42 min.

gives quite satisfactory results as exemplified by the original image in Fig. 11, which was obtained with a regular dot pattern and has very dense fringes, and by its Fourier-filtered counterpart shown in Fig. 12. The texture is smoothed, and even some of the curvilinear defects visible all over the image are dampened or even completely removed.

In the presented processed images the black areas surrounding the image itself are those for which no output was calculated. In the case of the Fourier filter this is due to the fact that the center of the mask cannot be placed near the boundary of the image. The same holds for all image enhancement methods in which masks are used, among them the Markov method as well as for the adaptive median filter. In the subsequent images all the unprocessed pixels are always shown in black.

Let us now examine the results of image enhancement of the three other methods. First, the results for each method are discussed individually. Then, the results obtained with all the three methods are compared by means of the example image of the beam of Fig. 23.

The parameters of the image enhancement methods and the calculation times are specified in the respective figure captions.

The adaptive median filter

This filter smoothens the texture of the fringes and also eliminates the reflexes to some extent. It leaves some of the fine granularity in the filtered image, as shown in Figs. 14

and 25. This remaining granularity can be further removed by other image enhancement methods, as shown for the membrane method in Fig. 27.

The adaptive median filter is the fastest of all the methods considered in this paper.

The Markov method

A satisfactory smoothing of the grey level function can also be obtained by using the method based on the estimated Markov model. The results are illustrated by three examples. The original image for the enhanced image in Fig. 15 is a specklogram of a beam with random dot speckles, characterized by a very poor quality, with very irregular variability of the grey level, and many reflexes generated in the optical system. The enhanced counterpart of the image in Fig. 13 is shown in Fig. 15. The second and third examples of the image enhancement by the Markov method are shown in Figs. 18 and 24. Both of these images were obtained from the originals of relatively good quality and with clearly defined fringes.

In the image of Fig. 24 only the window containing the object, and not the background, has been enhanced, to let the Markov method correctly estimate the stochastic parameters of the grey level field representing the object (this is in agreement with the explanations in Section 2.2.4). Leaving aside the problem of separating the interesting part of the image from all the rest, one can also get satisfactory results when the background is inside the processed window, as exemplified by Fig. 15. However, lack of theoretical justification concerning the stochastic parameters estimation in this case makes such a result unreliable.

In all the cases the proposed method leads to a visible improvement of the image by smoothing the texture and blurring the reflexes. This result, however, is achieved at a cost of some distortion of the contours of the object.

The weak membrane method

Image enhancement based on the membrane model ensures very good smoothing of fringes and elimination of irregularities of the grey level function. However, it can lead to the change of shape or even to vanishing of the fringes, and to the distortion of the contours of the object. This happens because the method makes it easy to obtain a very large degree of smoothing. Examples of enhancement effects are shown by the four following images: the beam in Fig. 16, the image of Fig. 20 with a very grainy original, the image of Fig. 22 the original of which has a very poor contrast, and the beam in Fig. 26.

Enhancement method using the membrane model ensures a visible improvement of quality of the images. The ability of the membrane to break (Section 2.3) proves its usefulness for preserving sharp edges and isolating light reflexes. This can be observed in particular in Fig. 16[9]. The scaling parameter $\lambda = 8$ is particularly large, and the grey

[9] This image was obtained with the version of the method with enhanced sensitivity to skewed edges ([19]).

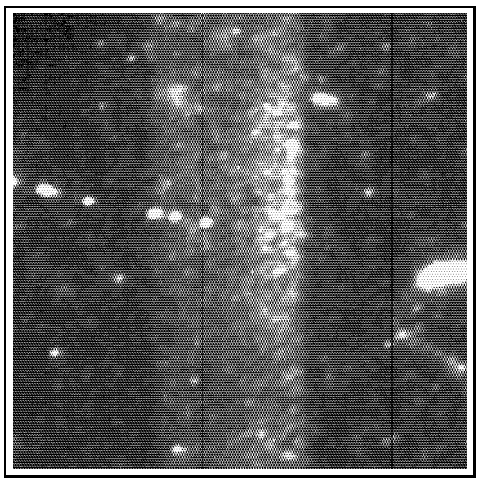

Fig. 13. Longitudinal displacement of a cantilever beam - the original 256×256 image.

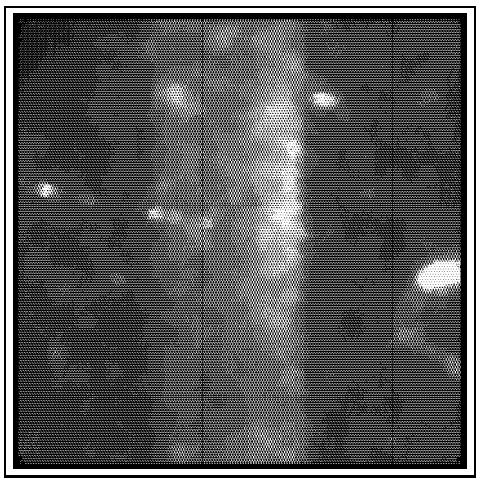

Fig. 14. Image of Fig. 13 after a sequence of three adaptive median filterings; the sizes of consecutive masks are 7×7 and twice 9×9. Time ≈ 0.8 min.

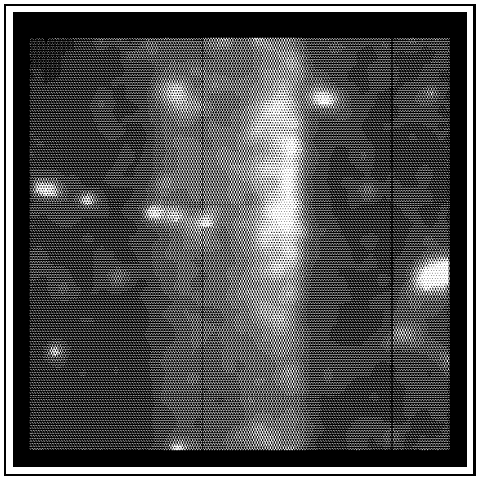

Fig. 15. Image of Fig. 13 enhanced with the Markov method. Signal/noise ratio = 0.9, edge threshold = 150, smoothing = YES. Time ≈ 1.3 min.

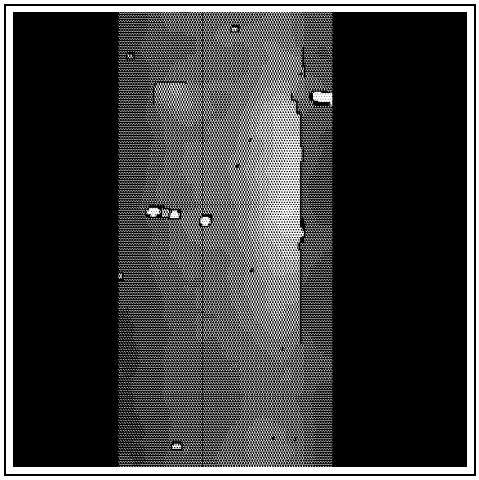

Fig. 16. Image of Fig. 13 enhanced with the membrane method; $\lambda = 8$, $h_0 = 64$. Membrane breaks marked with black pixels. Processed window 120×256. Calculation time for the window ≈ 11 min; for the whole image it would be ≈ 23 min.

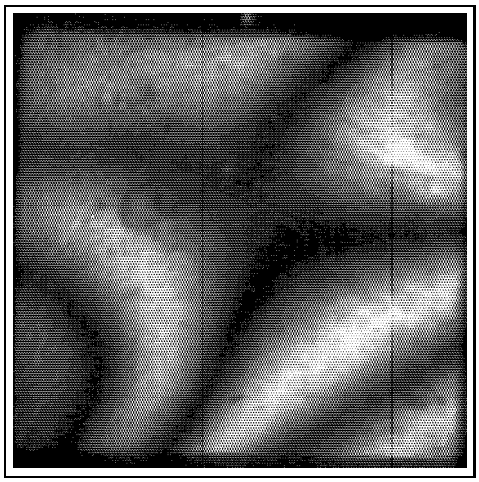

Fig. 17. First example of the rotation and translation of a rigid object - the original 256×256 image.

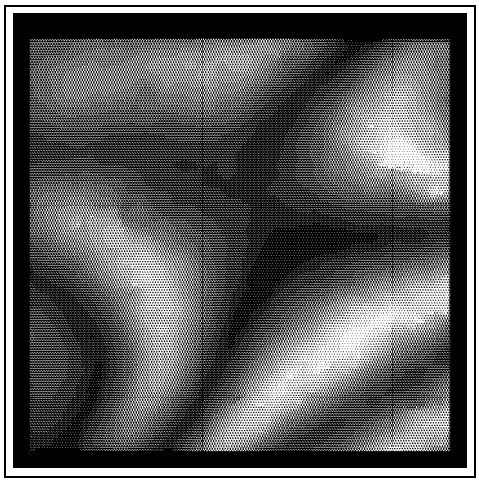

Fig. 18. Image of Fig. 17 enhanced with the Markov method. Signal/noise ratio = 0.9, edge threshold = 45, smoothing = YES. Time $\approx$ 1.2 min.

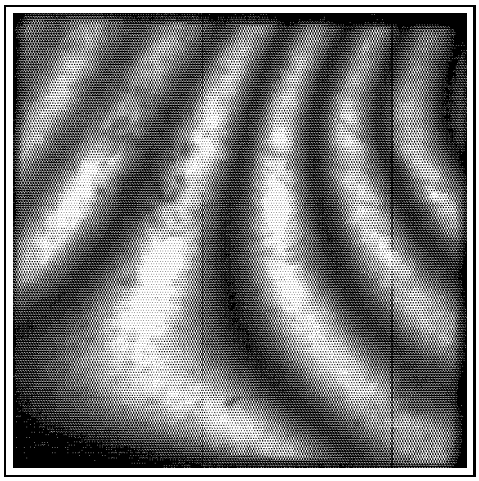

Fig. 19. Second example of the rotation and translation of a rigid object - the original 256×256 image.

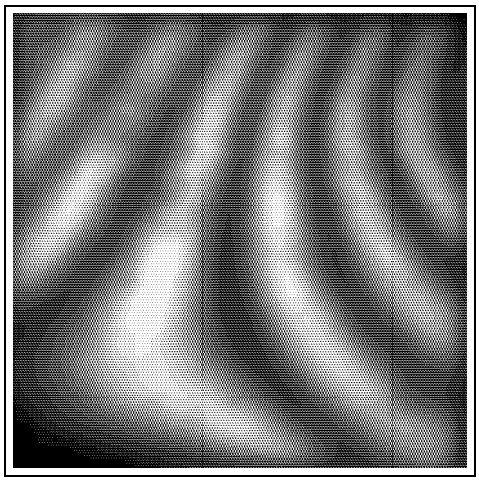

Fig. 20. Image of Fig. 19 enhanced with the membrane method; $\lambda = 4$, $h_0 = 128$. Time $\approx$ 18 min.

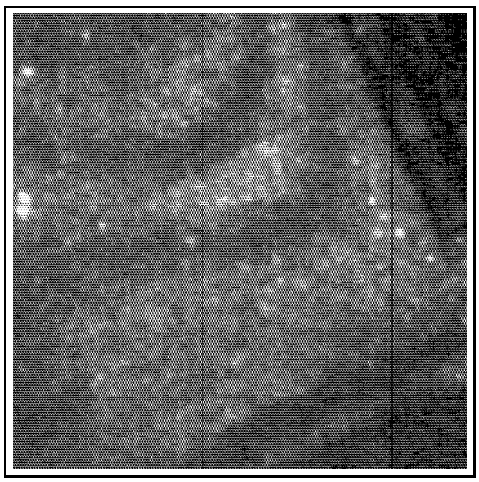

Fig. 21. Displacement of a buckled plate - the original 256×256 image.

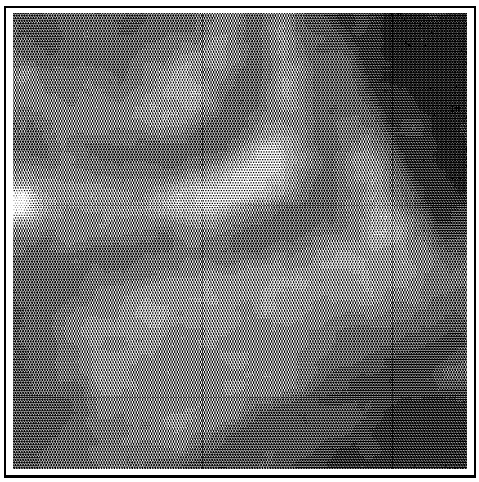

Fig. 22. Image of Fig. 21 enhanced with the membrane method; $\lambda = 8$, $h_0 = 128$. Time $\approx$ 20 min.

level function is effectively smoothed. It can be observed that the right-hand side edge of the beam with stronger contrast is well preserved, although the remaining contour of the beam is blurred. The three evident false artefacts (reflexes) in the middle part of the image are surrounded by the membrane breaks, so they do not interfere with the grey level function values in their vicinity.

Comparison

The effects of image enhancement are discussed with reference to images in Figs. 23-27, and to their cross-sections shown in Figs. 29-33 which were done along a chosen row, as shown in Fig. 28.

The original image for the comparison is a very typical fringe image obtained with random speckles: the specklogram of a cantilever beam shown in Fig. 7. The fringes in this image are quite clear, but the texture is very grainy and parts of the image are corrupted by reflexes and overexposure.

The three methods have led to the smoothing of the grey level function, but in the case of the Markov and the membrane methods this has been done at a cost of diminishing the contrast of the image (Figs. 24, 30 and 26, 32). The adaptive median filter preserved the contrast, but did not make the grey level function quite smooth (Figs. 25 and 31). This effect can be partly removed by further filtering, as illustrated by Figs. 27 and 33, at the expense of some more processing time.

The results obtained with the image enhancement method using the estimated Markov

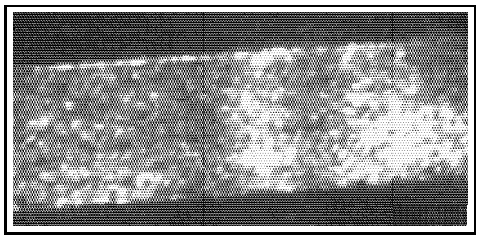

Fig. 23. Transversal displacement of a cantilever beam, red component - the original 256×120 image.

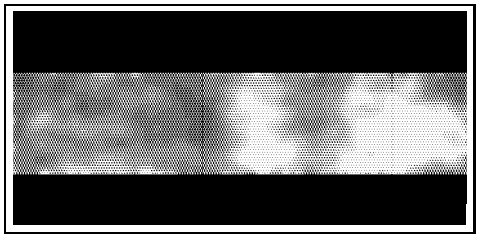

Fig. 24. The image of Fig. 23 enhanced with the Markov method. Signal/noise ratio $= 0.9$, edge threshold $= 150$, smoothing = YES. Time ≈ 0.5 min. A window containing no background has been processed.

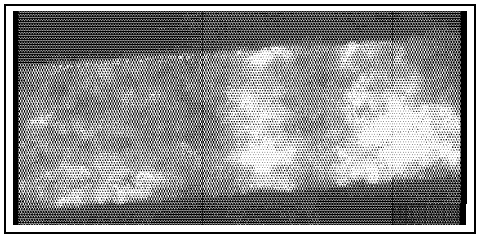

Fig. 25. The image of Fig. 23 enhanced with a sequence of two adaptive median filters, with masks 7×7 and 9×9. Time ≈ 0.24 min.

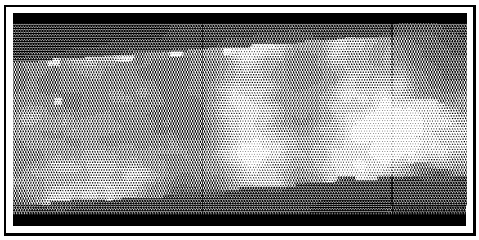

Fig. 26. The image of Fig. 23 enhanced with the membrane method; $\lambda = 4$, $h_0 = 64$. Time ≈ 10 min. The processed window is slightly smaller than the original image.

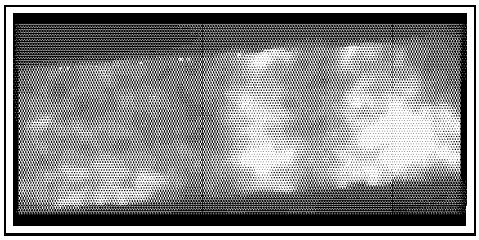

Fig. 27. The image of Fig. 25 enhanced with the membrane method. $\lambda = 1.2$, $h_0 = 64$. Time ≈ 1.2 min. The fine texture left by the adaptive median filter is partly removed.

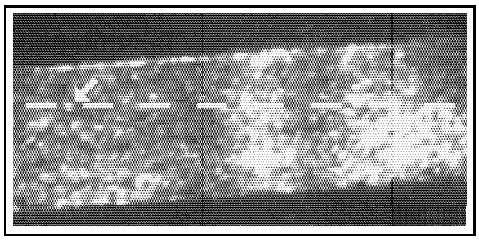

Fig. 28. Image of Fig. 23. The cross-sections of the grey level functions along the row marked with a broken line are shown in the following Figures. The section runs across an isolated reflex indicated by an arrow.

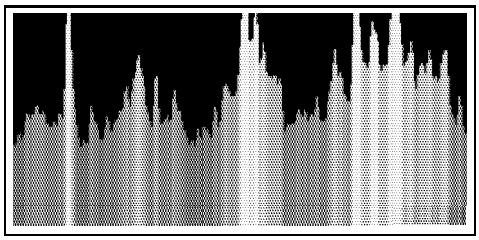

Fig. 29. The cross-section of the grey level function of the original image (Fig. 28). Height and brightness of bars represent grey levels in subsequent pixels (grey level $\in \langle 0, 255 \rangle$ vs. pixels $\in \langle 0, 255 \rangle$).

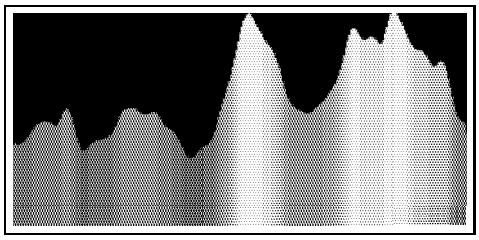

Fig. 30. The cross-section of the grey level function of the image from Fig. 28 enhanced with the Markov method (Fig. 24).

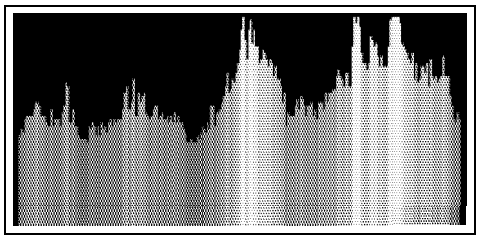

Fig. 31. The cross-section of the grey level function of the image of Fig. 28 after adaptive median filtering (Fig. 25).

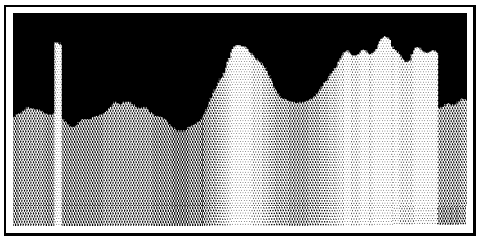

Fig. 32. The cross-section of the grey level function of the image of Fig. 28 enhanced with the membrane method (Fig. 26). The isolated light reflex (marked in Fig. 28) is separated.

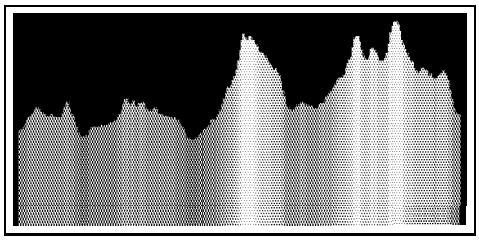

Fig. 33. The cross-section of the grey level function of the image from Fig. 28 enhanced with the adaptive median filter (Fig. 25), and then with the membrane method (Fig. 27).

model are probably the best in a general case. However, this particular method requires exclusion of the background from the image to be enhanced, and can make it difficult to recover the whole area of the object of interest.

The method using the membrane model does not have this drawback, and additionally it presents a possibility of maintaining sharp edges in the image and separating some artefacts which clearly do not conform with the local variation of the grey level function (see especially Fig. 32). This method, however, reduces the contrast of the image more than is the case with the remaining methods. Moreover, the calculation time of the membrane method is the longest.

Summary of comparison

The above presentation of the enhancement results can be summarized as follows:

- The adaptive Fourier filter fails to detect the direction of sparse fringes and gives unacceptable results.
- The adaptive median filtering gives satisfactory results in the shortest time, but leaves some unwanted fine texture in the image. This texture, however, can be removed to some extent by the membrane method as well as by the Markov method.
- The results of the Markov and the membrane methods of image enhancement are similar. The membrane method having a very strong potential of smoothing the grey level function tends to reduce the fringe contrast to a higher degree than the Markov method does.
- The membrane method preserves sharp edges between an object and its background and separates some high-contrast false artefacts in the image, while the Markov method for best results should not be used for processing the background in the image.
- The calculation times for the three methods, measured for a 256×256 image and typical operating parameters can be roughly estimated as:
  median : Markov : membrane $\approx$ 0.5 : 1 : 20 min. Calculation time is not a decisive factor as long as laboratory analysis of physical phenomena which produce fringe images is concerned. However, times longer than few minutes make a method less attractive for the end-user.

The main problem which has not been adequately solved is that together with rejection of high-frequency noise, the contrast of fringes is reduced. The method of contrast equalizing proposed in the Section 3 is a trial of overcoming this problem, but the preliminary results show that more attention should be paid to this problem in future.

Further work on the enhancement methods of sparse fringe images is necessary; however, the methods developed up to now offer a powerful set of tools from which one can choose the most suitable one for a particular task.

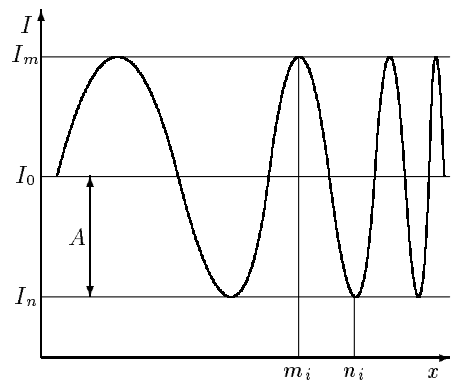

Fig. 34. Cross-section along the axis x of the grey level function in a fringe image with constant amplitude A, background I_0, and contrast. m_i and n_i - ridge and valley of a fringe i; I_m and I_n - maximum and minimum of the grey level.

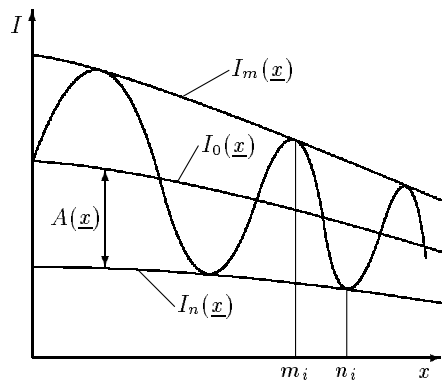

Fig. 35. Cross-section along the axis x of the grey level function in a fringe image with variable amplitude $A(\underline{x})$, background $I_0(\underline{x})$, and contrast. m_i and n_i - ridge and valley of a fringe i; $I_m(\underline{x})$ and $I_n(\underline{x})$ - upper and lower surfaces of a fringe image (see Section 3.2).

3. Contrast and Background Equalizing (LC)

3.1. The Concept

Numerous problems result from the fact that in the fringe images both the contrast and the brightness are neither uniform nor explicitly given. An 'ideal' fringe image would be the one with uniform and large contrast, and with uniform brightness in the whole field of view. Let us make a cross-section of the grey level function along a line perpendicular to a dominating direction of fringes in the image. Without loosing generality assume that this line is given by the equation $y = const$ (Fig. 34). In the graph of Fig. 34 the background grey level I_0[10], the amplitude A, the contrast γ are all constant, and the maximum and minimum grey level values I_m and I_n are the same for all the fringes. In accordance with Fig. 34 one obtains ([11])

$$A = (I_m - I_n)/2 \tag{24}$$

$$I_0 = (I_m + I_n)/2 \tag{25}$$

$$\gamma = A/I_0 \tag{26}$$

The grey level I at a given point $\underline{x}$ of the image ($\underline{x} \equiv (x, y)$, $\underline{x} \in \underline{X}$, where $\underline{X}$ is the image domain) depends only on the phase $\varphi = \varphi(\underline{x})$ and, can be expressed as [9, 11, 15]

$$I(\underline{x}) = I_0[1 + \gamma \cos(\varphi(\underline{x}))] \tag{27}$$

[10] In this section, *background* denotes *average grey-level of fringes* , and does not denote the part of the image not taken by the object with fringes, as in other sections.

In the real life images, both the contrast and the background level are variables which depend on the position in the image

$$I(\underline{x}) = I_0(\underline{x})[1 + \gamma(\underline{x}) \cos(\varphi(\underline{x}))] \tag{28}$$

One can regard the real life image defined by Eq. (28) as an image obtained by *deforming* an image with the constant background level I_0 and contrast γ (Eq. (27)). This is equivalent to replacing these constants by the variables $I_0(\underline{x})$ and $\gamma(\underline{x})$. It should be stressed that it is the *grey level function* of the image that is deformed, and not the *shape* of the objects (fringes) in the image, as in [12, 14].

Initially, one has the real, *deformed* image. The notion *deformed* image will denote this given image. The corresponding image which has the constant background level I_0 and contrast γ will be called the *equalized* image.

An example of a cross-section of the grey level function of a *deformed* image is shown in Fig. 35 (the cross-section was obtained in the same way as in Fig. 34).

Our task is to find the *equalized* image having the *deformed* one. This operation will be called the *equalization* of an image. In order to *equalize* an image one has to find its contrast and background functions: $\gamma(\underline{x})$ and $I_0(\underline{x})$ (or any two out of the three related functions: contrast, grey-level, and amplitude), and to replace them with constant values[11].

The most important information contained in the image is the phase $\varphi(\underline{x})$. It is worthwhile to note that if the accurate values of $\gamma(\underline{x})$ and $I_0(\underline{x})$ were known, then the phase could be directly calculated from the image with Eq. (27). However, as it will be seen in Section 3.4, at the present development stage of the algorithm such a calculation would not be sufficiently accurate.

The most straightforward way of finding the constant background level and the contrast of an equalized image (Fig. 34) is to find the maximum and minimum grey levels: I_m and I_n, and to use Eqs. (24)-(26). We shall do this for the deformed image given in Fig. 35.

For the purposes of further calculations the functions are introduced which are the variable counterparts of the constant values I_m and I_n, that is $I_m(\underline{x})$ and $I_n(\underline{x})$. The procedural details for this approach are worked out in the next Section.

3.2. Upper and Lower Surfaces: Definition

Let us rewrite Eqs. (24)-(26) with the constant values replaced by the variable ones

$$A(\underline{x}) = (I_m(\underline{x}) - I_n(\underline{x}))/2 \tag{29}$$

$$I_0(\underline{x}) = (I_m(\underline{x}) + I_n(\underline{x}))/2 \tag{30}$$

$$\gamma(\underline{x}) = A(\underline{x})/I_0(\underline{x}) \tag{31}$$

[11] Obviously, $I_0 > 0$ and $\gamma \in (0,1\rangle$, as $I > 0$.

Elimination of $A(\underline{x})$ leads to

$$I_m(\underline{x}) = I_0(\underline{x})[1+\gamma(\underline{x})] \tag{32}$$

$$I_n(\underline{x}) = I_0(\underline{x})[1-\gamma(\underline{x})] \tag{33}$$

The functions $I_m(\underline{x})$ and $I_n(\underline{x})$ are called the *upper* and the *lower* surface, respectively, of a fringe image with the grey level function expressed by Eq. (28). An example of these surfaces is shown in Fig. 35. If such surfaces could be found from a given deformed image, then the contrast and the grey level function could be calculated from Eqs. (29)-(31).

The only way of finding the upper (lower) surface of a given fringe image seems to be that of spanning it by interpolation between the fringe ridges (valleys) which form a set of lines in the image domain. There are two basic problems with this idea: how to localize the interpolation nodes (or lines, as the case is a 2D one), and how to choose an appropriate interpolation method.

The interpolation lines coincide with the fringe ridges and valleys, because the upper (lower) surface of the fringe image is tangent to the graph of the grey level function along the fringe ridges (valleys). In the equalized image the fringe ridge (valley) corresponds to the maximum of the grey level m_i (minimum n_i) and is easy to find. However, in the deformed image the fringe ridge and maximum of the grey level do not coincide, as it can be seen in Fig. 36.

A ridge (valley) in the deformed image cannot be defined without reference to the equalized image. This is an important observation from the point of view of the interpretation of fringe images. In the case under consideration, the above observation presents a major obstacle. In this preliminary study the difficulty has been overcome by the use of an approximation. It was assumed that the difference between the maximum (minimum) and the fringe ridge (valley) is negligible, which is not far from truth for images with small upper (lower) surface gradients. An accurate solution could be found iteratively by considering the maxima (minima) of the grey level in the first equalized image as the new interpolation lines in the input image for the next equalization step and so on. This procedure has not been used here, as it turned out that the inaccuracies caused by the distortions in the given deformed images were much larger than those resulting from the approximation (compare Sec. 3.4).

The choice of the interpolation method remains arbitrary. All that can be said about the upper and lower surfaces of the deformed image is that they satisfy Eqs. (32) and (33), and that these equations contain unknown functions $I_0(\underline{x})$ and $\gamma(\underline{x})$. The interpolation method has to make it possible to span a smooth two-dimensional surface between sparsely positioned, not necessarily continuous lines. The surface has to conform to these lines in the sense of a minimum of some error function, because the lines are distorted by noise in the image. It would be desirable to use an interpolation-extrapolation method, as the surface should be built over the whole image domain, and not only 'between the lines'.

The method currently in use is presented in Section 3.3. Some examples are shown

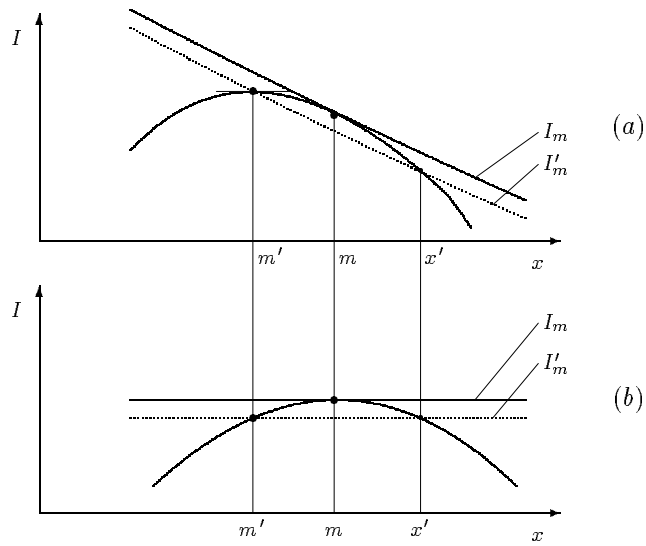

Fig. 36. Fringe ridge and maximum of the grey level function; (a) in a deformed image: ridge at $x = m$, maximum at $x = m'$; (b) in an equalized image: ridge and maximum coincide at $x = m$. The approximate upper surface I'_m passing through the grey level maximum at $x = m'$ in the deformed image (a) lies under the accurate surface I_m and crosses the grey level function graph at $x = m'$ and $x = x'$.

in Section 3.4.

3.3. Finding Upper and Lower Surfaces

At present, the lower and upper surfaces are found in a semi-automatic way. Let us now fix our attention on finding the upper surface. The first step is to find the locations of the fringe ridges. This task is usually much easier if a filtered image is used (the 'weak membrane' filter with very large scale λ is a good proposition – see Section 2.3). The pixels of the ridges will serve as the interpolation nodes. The ridges are represented by sets of pixels. The pixel ordering information is not used.

Because of the limited quality of the images, for the start we chose the manual way of finding fringe ridges; the automatic ridge-following algorithms would be quite suitable, but finding good starting and ending points and excluding bad fragments seems difficult to automatize. Probably a semi-automatic procedure would have been the best solution.

The surface finding algorithm is an interpolation-extrapolation 2D algorithm. The main problem with this algorithm is to find balance between the two following contradictory requirements. On one hand, the surface should be smooth, with the ability to extrapolate out of the region occupied by fringes, according to the tendency from inside

that region. On the other hand, the ridges and valleys can be quite uneven, and the surfaces should follow their shape, which typically makes interpolation algorithms fall into instabilities between the nodes. The proposed algorithm is a tradeoff between stability and closeness to data.

It is understandable that good results can not be expected in images or image regions with too few fringes.

In the below sketch of the algorithm it will be assumed that the *upper* surface is found by interpolation and extrapolation over the fringe ridges[12].

Stage 1 A privileged direction (PD) is chosen – horizontal (H) or vertical (V). If the majority of fringe ridges are horizontal, PD will be vertical, and vice versa.

In each row ($PD = H$) or column ($PD = V$) the centres of the fringes become the primary nodes. It is assumed in the sequel that $PD = H$.

Stage 2 The grey level function between the primary interpolation nodes is interpolated along PD (along rows) with parabolic splines. The grey level values are also extrapolated outside the intervals between the primary nodes on the basis of the outermost intervals. In this way new grey level values are found in all the pixels of the fringe image. The pixels with these new values become the secondary nodes, which now cover the whole area of the image.

Stage 3 In the direction perpendicular to PD (along columns) the third degree polynomial fitting is performed, based on the mesh of the secondary nodes. This fitting is carried out in the columns separated by the distance *step*. The third order nodes are found on the fitted curves, also at a distance *step* from each other.

Stage 4 The mesh of size $step \times step$ of the third order nodes formed in Stage 3 is filled in with ruled surface patches. These patches form the sought surface.

In this way, the image grey levels are interpolated with a piecewise-linear[13] approximation of the curvilinear surface, which is a 3rd degree surface along the dominating direction of the fringes, and the 2nd degree spline surface in the perpendicular direction. Hence, the surface is more 'even' in that direction for which there is less data. Extrapolation outside the region occupied by the fringes is also performed.

3.4. Examples of Equalizing Fringe Images

The results obtained with the presented algorithm are not yet entirely satisfactory; therefore, we consider it suitable to give one good example and one worse. To make the presentation more encouraging, the good one will be presented first.

[12] The algorithm was developed for EPSILON ARG by Tomasz Lekszycki and Andrzej Zacharski from the Institute of Fundamental Technological Research, Polish Academy of Sciences.

[13] Because the filled-in patches are ruled surfaces.

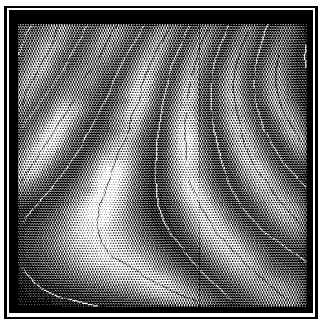

Fig. 37. First test image for equalization; dimensions 240 × 240; 256 grey levels; marked fringe ridges and valleys.

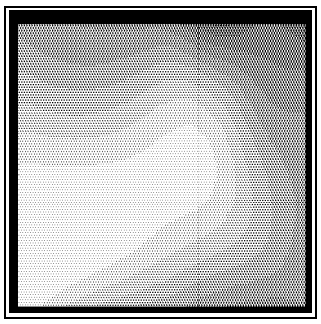

Fig. 38. Upper surface of the image from Fig. 37; $step = 3$.

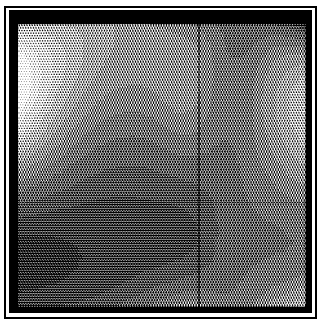

Fig. 39. Lower surface of the image from Fig. 37; $step = 3$.

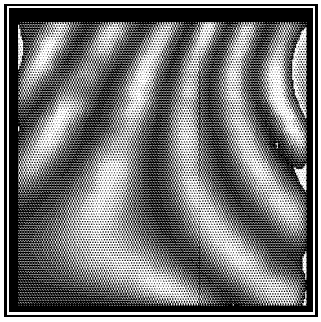

Fig. 40. Image of Fig. 37 with contrast equalized to 0.80 and background to 115.

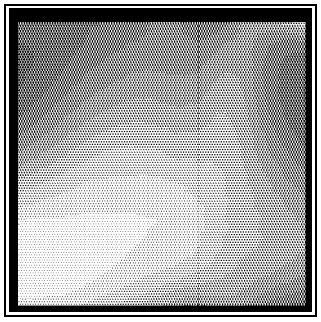

Fig. 41. Contrast of the image from Fig. 37 ranging from 0.32 to 0.97; black corresponds to 0.00, white to 1.00.

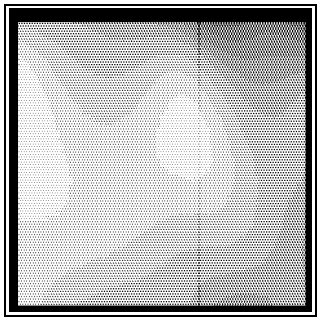

Fig. 42. Background of the image from Fig. 37 ranging from 53 to 138.

One of the clearest images in Section 2.4 is that in Fig. 20. The same image after membrane enhancing is shown in Fig. 37. The subsequent figures show the upper and lower surfaces (Figs. 38 and 39), contrast (Fig. 41), background (Fig. 42), and the equalized version (Fig. 40) of the image in Fig. 37.

Severe defects are visible in the equalized image (Fig. 40) near the boundaries: the grey scale was exceeded which manifests itself in wraparound of the grey level.

Although the outer parts of the equalized image are corrupted, a significant improvement of the contrast and brightness uniformity in the interior of the image was obtained.

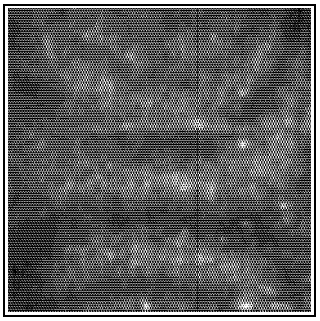

Fig. 43. Second test image for equalization and before enhancement; dimensions 120×120; 256 grey levels.

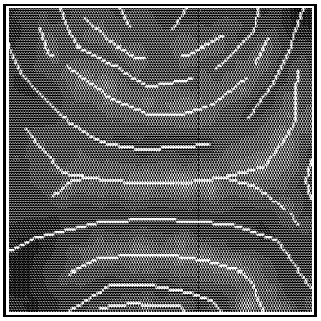

Fig. 44. Image of Fig. 43 after enhancing with the membrane method; $\lambda = 2$; $h_0 = 512$; marked fringe ridges and valleys.

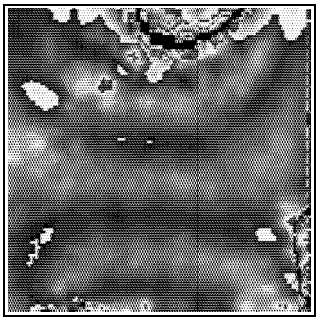

Fig. 45. The image from Fig. 44 with the contrast equalized to 0.80 and background to 60.

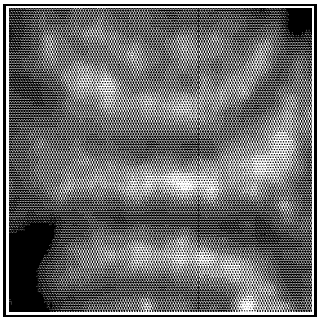

Fig. 46. Image from Fig. 44 with the grey scale linearly extended and shifted.

As the second example, an image with a smaller number of fringes and worse contrast was chosen (Fig. 43). The original image is the red component of one of the experimental images obtained with the white-light random dot speckle method. The result of equalization in Fig. 45 is not as good as in the first example, as it was extremely difficult for the interpolation algorithm to fit the data closely and to avoid mutual crossing of the upper and the lower surface and the image grey level surface in the areas of low contrast and bad fringe quality.

Let us now consider Fig. 46. This figure presents the image of Fig. 44 modified by linear extension and shift of the grey scale in order to obtain maximum resemblance with the equalized image of Fig. 45.

Now, let us compare the modified image (Fig. 46) to the equalized one (Fig. 45).

Besides the absence of corrupted areas in the modified image, the fringe contrast is less uniform and the fringe ends are not so distinct as in the equalized image.

Note that in the image of Fig. 44 the horizontal linear defect and one of the bright light spots (in the direction SE with respect to the linear defect) visible in Fig. 43, were removed with the membrane method, by excluding the corresponding areas of the input picture from the data fitted with the membrane (advantage 5 in Section 2.3).

4. Conclusion

The paper discusses the problem of enhancing speckle fringe images used in the LWSM in the case of white light and random dot patterns. The most essential features of such images are the graininess of their texture and the sparsity of the fringes. For this reason typical fringe-oriented filtering methods relying on the directionality and repetitivity in the image do not give satisfactory results. Therefore, three other methods have been adapted and tested on a set of examples of fringe images which are representative for the LWSM. The analyzed methods of image enhancement are: the adaptive median filter, the method based on the estimated Markov model, and the method using weak membrane model. To the best of the authors' knowledge, the methods based on the estimated Markov model and on the membrane model have not been applied up to now to the analysis of the fringe images.

The three methods were found to perform acceptably well. The MRF and the membrane methods are the best at smoothing the texture. The median filter better preserves contrast, while leaving some fine-grain structure. The membrane method's property of preserving sharp edges and not letting high-contrast false artefacts deform the surrounding grey levels is useful, and its smoothing properties seem to be the strongest. However, this may be at a cost of pronounced contrast reduction. The MRF filter seems to balance the advantages and the drawbacks in a most desirable way. The greatest problem with this filter, however, is that the image cannot include the background in addition to the fringe-covered object.

The times of calculation for the three filters, referred to a hypothetical 256×256 image with typical parameters, could be roughly estimated as $0.5 : 1 : 20$ min on an AT 80486DX, 50MHz computer.

Additionally, a numerical method of equalizing and enhancing the contrast of a fringe image is introduced in this paper and evaluated. The preliminary results are encouraging, although it seems that more work must be done to make this method applicable to other tasks than simply enhancing images for presentation purposes.

The study on image equalization made it possible to define the difference between the true positions of the ridges and valleys of fringes and the positions of maximum and minimum of the grey level function in an image with variable contrast and background brightness.

Further work is necessary on how to avoide reduction of fringe contrast while removing the high-frequency noise from images. Nevertheless, the developed and presented filters and methods are capable of yielding satisfactory results in numerous cases.

Acknowledgments

The research was financed by the Committee of Scientific Research (KBN) under the Grant No 8 8055 91 02, in the period from May 1992 to April 1993.

References

[1] Besag J.: Spatial Iteraction and the Statistical Analysis of Lattice Systems, *Journal of Royal Statistical Society*, series B, 36, 192-236.

[2] Chiang F.P., Asundi A.: White Light Speckle Method of Experimental Strain Analysis, *Applied Optics* 18(4), 409-411.

[3] Hassner M., Sklansky J.: The Use of Markov Random Fields as Models of Texture, *CGIP*, 12, 357-70.

[4] Cross G.R., Jain A.K.: Markov Random Fields Texture Models, *IEEE Trans. PAMI*, 5(1). 25-39.

[5] Geman S., Geman D.: Stochastic Relaxation, Gibbs Distributions and the Bayesian Restoration of Images, *IEEE Trans. PAMI*, 6, 721-41.

[6] Besag J.: On the Statistical Analysis of Dirty Pictures, *Journal of Royal Statistical Society*, series B, 48, 259-302.

[7] Blake A., Zisserman A.: *Visual Reconstruction*, Cambridge, MIT Press.

[8] Kass M., Witkin A.: Analyzing Oriented Patterns, *CVGIP*, 37(3), 362-385.

[9] Ranson W.F., Sutton M.A., Peters W.H.: Holographic and Laser Speckle Interferometry, in: Kobayashi A. S.(Ed.): *Handbook on Experimental Mechanics*, SEM, Prentice-Hall.

[10] Chalmond B.: Image Restoration Using an Estimated Markov Model, *Signal Processing*, 15(2), 115-29.

[11] Creath K.: Phase Measurement Interferometry Techniques, in: Wolf E. (Ed.): *Progress in Optics*, Elsevier Science Publ., vol. 26.

[12] Kosiński W., Frischmuth B.: On a Family of Deformations in the Recognition Process (in Polish), in: Chmielewski L. and Kosiński W. (Eds.): Computer Modelling of Perception and Reasoning, part II, *IFTR Reports*, 42, 39-44.

[13] O'Gorman L., Nickerson J.V.: An Approach to Fingerprint Filter Design, *Pattern Recognition*, 22(1), 29-38.

[14] Li Z.C., Bui T.D., Tang Y.Y., Suen C.Y.: *Computer Transformation of Digital Images*, Singapore: World Scientific.

[15] Kujawińska M.: *Automatic Fringe Pattern Analysis in Optical Methods of Testing*, series Mechanics, vol. 138, Warsaw Technical University.

[16] Chmielewski L.: Report on Investigations of the 1D Filter Based on the Concept of the 'Weak String' (in Polish), EPSILON ARG Internal Report, Grant KBN 8 8055 91 02, Jun./Jul. 1992.

[17] Michalski B.: Estimation of the Images Subjected to Filtering (in Polish), EPSILON ARG Internal Report, Grant KBN 8 8055 91 02, Apr. 1992.

[18] Pieczyński W.: Statistical Image Segmentation, *Machine Graphics & Vision*, 1(1/2), 261-81.

[19] Chmielewski L. : Local Method of Length and Direction Estimation for Stepped Representations of Curves – Application to the 'Weak Membrane' Image Restoration Algorithm, *Machine Graphics & Vision*, 2(2), 123-142.

[20] Cudny W., Chmielewski L. : Light wave length measurement with a colour camera, *Machine Graphics & Vision* 2(3), 251-260.

[21] Kuriański A., Skłodowski M. : Enhancement of Speckle Images with the Use of Statistical Markov Field Models, *Machine Graphics & Vision*, 2(4), 309-338

[22] Kuriański A. : Markov Fields in Computer Image Analysis (in Polish), Proc. 2nd Seminar on Mathematical Methods of Fringe Image Analysis, organized by OC PTM, Częstochowa, Mar. 1993.

[23] Skłodowski M., Cudny W. : The White Light Wavelength Stepping Method, EPSILON ARG Internal Report, Grant KBN 8 8055 91 02, Oct. 1992 - Mar. 1993.

[24] Skłodowski M. and Cudny W. : Theory and Draft Algorithm for the Light Wavelength Stepping Method, *Machine Graphics & Vision*, 3(1/2).

[25] Kosiński W., Chmielewski L. : On Image Restoration with the Method of Deformed Plate and/or Membrane with the Loss of Continuity, in preparation.